The Mechanism of Cleavage of RNA Phosphodiesters by a Gold Nanoparticle Nanozyme

Joanna Czescik,[a, c] Fabrizio Mancin,[a] Roger Strömberg,*[b] and Paolo Scrimin*[a]

Abstract: The cleavage of uridine 3′-phosphodiesters bearing alcohols with pK_a ranging from 7.14 to 14.5 catalyzed by AuNPs functionalized with 1,4,7-triazacyclononane-Zn(II) complexes has been studied to unravel the source of catalysis by these nanosystems (nanozymes). The results have been compared with those obtained with two Zn(II) dinuclear catalysts for which the mechanism is fairly understood. Binding to the Zn(II) ions by the substrate and the uracil of uridine was observed. The latter leads to inhibition of the process and formation of less productive binding complexes than in the absence of the nucleobase. The nanozyme operates with these substrates mostly via a nucleophilic mechanism with little stabilization of the pentacoordinated phosphorane and moderate assistance in leaving group departure. This is attributed to a decrease of binding strength of the substrate to the catalytic site in reaching the transition state due to an unfavorable binding mode with the uracil. The nanozyme favors substrates with better leaving groups than the less acidic ones.

Introduction

The non-enzymatic hydrolytic cleavage of phosphate diesters is a continuously challenging endeavor for scientists because of their key role in connecting the constituent nucleosides of DNA and RNA.[1] Efficient catalysts could find an application in the fields of biotechnology, chemotherapy, and medicine. In the absence of catalysts, the phosphodiester linkage is exceptionally stable under physiological conditions.[2] Nevertheless, natural enzymes (nucleases) perform this job with high efficiency.[3] In the case of RNA, metal ions are often present in the catalytic site of these enzymes and play quite important roles in the catalytic process.[4] For instance, they prevent the electrostatic repulsion between negatively charged species, they are involved in the Lewis acid activation of the electrophile, in the increase of the concentration of deprotonated nucleophiles at neutral pH, and in facilitating the departure of the leaving group via pK_a reduction.[5] Elucidating the precise role of each contribution is a challenging task due to the interconnectedness of each process. By summing-up all of them, rate accelerations approaching 15–16 orders of magnitude have been estimated, not much different from those observed for nucleases.[5,6]

Numerous studies have shown that bimetallic catalysts are far better than their mononuclear counterparts.[7] Two metal ions may perform complementary tasks and optimize catalyst-substrate interactions. Multimetallic catalysts are more complex multivalent systems,[8] typically showing enhanced activity because of the introduction of a statistical amplification of the interactions with a substrate.[9] Metal ion-functionalized gold nanoparticles (AuNPs) belong to this category. Indeed, they proved to be rather efficient catalysts for the cleavage of phosphodiesters, including RNA model substrates, and DNA as well.[10] They are self-assembled supramolecular systems in which a cluster of gold atoms is coated with a passivating monolayer, which, for this application, is functionalized with metal ion complexes.[11] For their mode of action, and catalytic efficiency (up to 5–6 orders of magnitude rate acceleration with model substrates) they have been dubbed *nanozymes*[12] and are among the most efficient catalysts reported so far.

Commonly utilized, simple RNA model substrates are usually characterized by the presence of efficient leaving groups and are devoid of the nucleobases. The most used one is 2-hydroxypropyl p-nitrophenyl phosphate, **HPNP** (Figure 1).[13] Good leaving groups require very little (if any) protonation to depart from the substrate contrary to phosphate diesters of nucleic acids bearing a poorly acidic 5′-nucleoside.

In order to assess the efficiency of an artificial catalyst more challenging substrates must be studied, including those with a poor leaving group.[14]

A universal, accepted mechanism does not appear to exist for the metal ion-promoted cleavage of RNA model substrates.[15] The mechanistic studies are also complicated by the fact that similar kinetic evidence can concurrently support different mechanisms.

[a] *Dr. J. Czescik, Prof. Dr. F. Mancin, Prof. Dr. P. Scrimin*
Department of Chemical Sciences
University of Padova
Via Marzolo, 1 – 35131 Padova (Italy)
E-mail: paolo.scrimin@unipd.it

[b] *Prof. Dr. R. Strömberg*
Karolinska Institutet
NEO, 14157 Huddinge (Sweden)
E-mail: roger.stromberg@ki.se

[c] *Dr. J. Czescik*
Current address:
School of Life and Health Sciences
Aston University
B4 7ET Birmingham (UK)

Supporting information for this article is available on the WWW under https://doi.org/10.1002/chem.202100299

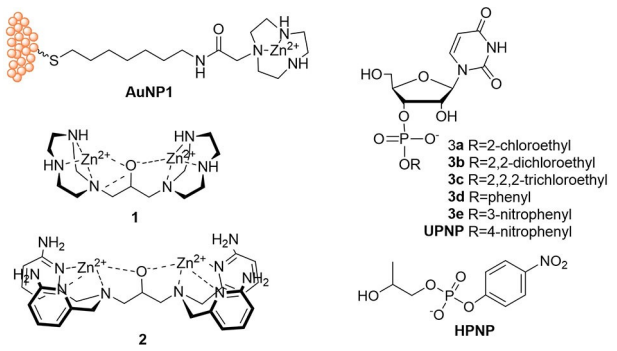

Figure 1. Catalysts and substrates discussed in this work.

Indeed, metal ions can enhance both the nucleophilic attack and leaving group departure following a general base or acid catalysis or even a bifunctional general base-general acid catalysis. Moreover, the mechanism also depends on the acidity of the metal-coordinated water molecule, the strength of the metal ion-substrate complex and the nature of the leaving group.[16] Accordingly, subtle changes within these parameters can significantly alter the resulting mechanism and, ultimately, the reaction rate. In addition, nucleobase-functionalized phosphates (as those present in RNA and DNA) may influence the interaction with the catalyst taking advantage of the ability of some of them to interact with the metal ion possibly altering the conformation of the complex.[17]

Our previous studies on **HPNP** hydrolysis catalyzed by AuNPs functionalized with 1,4,7-triazacyclononane, TACN, Zn(II) complexes revealed that the catalytic contribution could be attributed to nucleophilic activation as well as to Lewis acid catalysis.[13,18,19] Despite being one of the best catalysts reported for phosphate diester cleavage, no study regarding the role of the leaving group departure in AuNPs catalysis has been reported so far. Herein we report our studies on the hydrolysis of uridine 3′-phosphodiesters bearing alcohols with pK_a ranging from 7.14 to 14.5 using as the catalyst, the best Zn(II)-based nanozyme reported to date, for the cleavage of the RNA model substrate, **HPNP**.[13] We have also investigated how the uracil moiety present in the substrate affects its interaction with the catalyst and, ultimately, its catalytic efficiency. Our results were additionally compared with those reported for other dinuclear Zn(II)-based catalysts to unravel similarities and differences between them and our nanoparticles. The aim was to obtain a more comprehensive understanding of the mechanism of the reaction and elucidate the source of catalysis with these nanozymes.

Results and Discussion

The transesterification of UPNP

The gold nanoparticles we have used for our study (**AuNP1**, Figure 1) feature in the coating monolayer, a terminal TACN, as the ligand for Zn(II) complexation in situ. The mode of action of this catalyst requires the cooperation between two metal ions.[18,19] Cooperativity between two Zn(II) complexes has been shown to be favored by the presence of the amide group in the tether connecting TACN to the gold cluster.[13,20] In the passivating monolayer N-H···O=C H-bonds are formed leading to a more tightly packed structure.[20,21] Furthermore, the hydrocarbon chain ensures a hydrophobic environment resembling that of enzymatic active sites, which stabilizes the electrostatic interactions as well as desolvates nucleophiles. In the kinetic studies, the concentration of nanoparticles reported refers to the concentration of the TACN ligand present on their monolayer. This allowed us to evaluate the role of the metal complexes independently of their number on each nanoparticle.

To assess the difference in behavior between **HPNP** and uridine 3′-phosphodiesters, we first ran kinetics using the very reactive uridine 3′-p-nitrophenyl phosphate (**UPNP**). Under Michaelis-Menten conditions (i.e. excess substrate over catalyst), to determine the relevant kinetic parameters, we obtained the graph reported in Figure 2A. Instead of showing the saturation profile typical of an enzyme-like catalyst, the rate reached a maximum

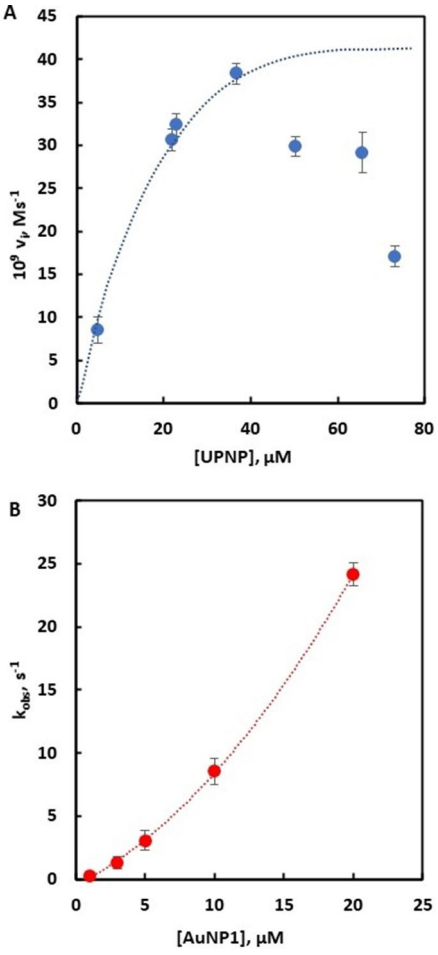

Figure 2. A. Initial rate vs **UPNP** concentration profile for the cleavage process catalyzed by **AuNP1**. The dotted line represents the fitting of the first four points with the Michaelis-Menten equation. Conditions: [**AuNP1**] = [Zn(II)] = 5.0×10^{-6} M, [HEPES] = 0.01 M, pH 7.5, 25 °C. B. Observed rate constant for the cleavage of **UPNP** at increasing **AuNP1** concentration. The dotted line is meant exclusively to guide the eye. Conditions: [**AuNP1**] = [Zn(II)], [HEPES] = 0.01 M, [**UPNP**] = 3.0×10^{-5} M, pH 7.5, 25 °C.

followed by a relatively sharp decrease. Thus, the curve obtained for **UPNP** indicates that, in the presence of **AuNP1** (at [**AuNP1**] = 5.0×10^{-6} M), when [**UPNP**] $>3.7\times10^{-5}$ M, the substrate starts inhibiting the reaction. The same phenomenon can be observed by running kinetics at constant **UPNP** concentration and increasing [**AuNP1**]. In this case (Figure 2B) the graph shows and upward curvature indicative of enhanced performance as the [catalyst]/[substrate] ratio increases. From the Michaelis-Menten analysis of the first portion of the curve (up to [**UPNP**] = 37 μM) for **UPNP** cleavage catalyzed by **AuNP1** (Figure 2A) we obtained the relevant kinetic parameters reported in Table 1. Although this analysis should be taken with some caution due to the competing inhibition process, some interesting observations can be made. First, k_{cat} is higher for **HPNP** than for **UPNP** (ca 13-fold).

Second, the k_{rel} (k_{cat}/k_{uncat}) values indicate a 34-fold acceleration of the cleavage of **UPNP** vs almost one million-fold for **HPNP** compared to the spontaneous, uncatalyzed process for the two substrates. Nevertheless, k_2 (k_{cat}/K_M) is higher for **UPNP** than for **HPNP**. The better performance of **UPNP**, in terms of second order rate constant, derives from a far lower K_M for this substrate that amounts to an almost 20-fold higher binding constant to the monolayer compared to that of **HPNP**. The above data suggest that **UPNP** binds to the TACN–Zn(II) complexes on the nanoparticle not only through the coordination of the phosphate but also through the uridine moiety. Binding of uridine to Zn(II) complexes is well known and occurs through the deprotonated imide nitrogen.[17] Lönnberg has shown that polynuclear catalytic complexes interact with the uridines of UpU and that at least a third metal ion is necessary to cleave the phosphate in a 1:1 complex.[22] This double interaction occurring on the nanoparticle surface increases the overall binding constant. However, the binding of the nucleobase to a nearby Zn(II) complex makes it unavailable for cooperating in the cleavage of the substrate. We have shown that phosphate diesters (but not triesters)[23] cleavage by TACN–Zn(II) complexes requires a dinuclear catalytic site.[10,12,18,19] As the concentration of **UPNP** increases, dinuclear catalytic sites become less and less available and the catalytic performance of the catalyst decreases (downward curvature of the graph of Figure 2A). The ability of uridine to bind to the monolayer could be confirmed in inhibition experiments using **HPNP** as the substrate. The K_i obtained (1.3×10^{-3} M, see Supporting Information) indicates that uridine binds to the Zn(II) complexes on the nanoparticle although with a slightly weaker binding constant than a phosphate diester.[24] With the same substrate, inhibition by dimethylphosphate leads to a $K_i = 7.6\times10^{-4}$ M. The effective molarity of the intramolecular binding process, due to the contemporary presence of the phosphate and uridine, $EM = K_{i,DMP}\times K_{i,uridine}/K_M$, is ca. 33 mM. This is less than what predicted by Mandolini for positive cooperativity (>60 mM).[25] This implies a non-optimal binding mode of **UPNP** to **AuNP1** not allowing to take full advantage of both binding units.

Richard and Morrows,[26,27] demonstrated enhanced catalytic efficiency of dinuclear catalyst **1** (Figure 1) for the cleavage of **HPNP** over **UPNP** (with respect to the uncatalyzed process) and concluded that facile access to the cationic catalytic site is sterically blocked for the bulkier **UPNP** substrate, an unlikely scenario for the nanoparticles because of the flexibility of the monolayer. In order to better understand the source of catalysis with **AuNP1**, we investigated the temperature dependence of the reaction rate for the cleavage of **UPNP** and compared the thermodynamic results with those available for **HPNP** (Table 2).[18] The analysis of Table 2 reveals that, while the entropic contribution to $\Delta G^{\neq}$ is lower for **UPNP**, the enthalpic contribution is higher. The lower $-\Delta S^{\neq}$ is likely the result of the absence of conformational freedom of the 2′-OH of **UPNP** locked in the tetrahydrofuran ring. On the contrary, the hydroxypropyl unit of **HPNP** can freely rotate thus populating also non-productive conformations. The movement towards the transition state for this substrate requires freezing of such a rotation. The higher $\Delta H^{\neq}$ could result from a partial detachment of **UPNP** from the bimetallic catalytic site connected to a non-appropriate geometry of binding associated with the presence of the uridine moiety as suggested also by the low EM determined above. Thus, for **AuNP1** catalysis, although the interaction of **UPNP** with the nanoparticle is stronger than that with **HPNP**, the formed complex is not the productive one leading to an efficient transesterification reaction. In order to properly orient the phosphate for the attack by the 2′-OH, part of that binding energy gain must be lost in the transition state. The stronger binding of **UPNP** to **AuNP1** also affects the pH vs rate profile of the reaction. Figure 3 shows that the rate of the catalyzed reaction goes up linearly with the increase of pH with slope = 1 and starts flattening at pH > 8. We have analyzed the curve considering one acidity constant (Equation 1):

$$k_{obs} = k_2[AuNP1](K_a/K_a + [H+]) \quad (1)$$

The best fitting gave a pK_a of 8.35 for the acidic species involved in the catalytic process, either a water molecule (base catalysis) or 2′-OH (nucleophilic catalysis) coordinated to Zn(II). In the case of **HPNP** the analogous pH vs rate profile is bell-shaped with two pK_a involved (7.8 and 9.2).[13] The second pK_a is typically associated with the deprotonation of a second Zn(II)-bound water

Table 1. Reactivity parameters for the **AuNP1** catalyzed cleavage of **UPNP** and **HPNP**.[a]

Substrate	UPNP[b]	HPNP[c]
k_{cat}, s^{-1}	0.0146	0.193
K_M, M	2.98×10^{-5}	5.80×10^{-4}
k_2 (k_{cat}/K_M), $M^{-1}s^{-1}$	490	333
$k_{rel} = k_{cat}/k_{uncat}$	34[d]	9.7×10^{5}[e]

[a] Conditions for UPNP cleavage: [**AuNP1**] = [Zn(II)] = 5.0×10^{-6} M, [HEPES] = 0.01 M, pH 7.5, 25 °C; for HPNP cleavage: [**AuNP1**] = [Zn(II)] = 2.5×10^{-5} M, [EPPS, buffer] = 1.0×10^{-2} M, pH = 7.5, 25 °C. [b] The analysis was performed on the first four points of the graph of Figure 2A. [c] Data from ref. 13. [d] $k_{uncat} = 4.3\times10^{-4}$ s^{-1}. [e] $k_{uncat} = 2.0\times10^{-7}$ s^{-1}.

Table 2. Thermodynamic parameters for **AuNP1** catalyzed cleavage of **HPNP** and **UPNP**.

Substrate[a]	$\Delta H^{\neq}$, KJ mol^{-1}	$\Delta S^{\neq}$, J mol^{-1}	$\Delta G^{\neq}$, KJ mol^{-1}[b]
HPNP	64.5	−53.3	81.1
UPNP	76.2	−28.4	85.1

[a] Data for **HPNP** from ref. 18, for **UPNP** this work. [b] T = 313 °K.

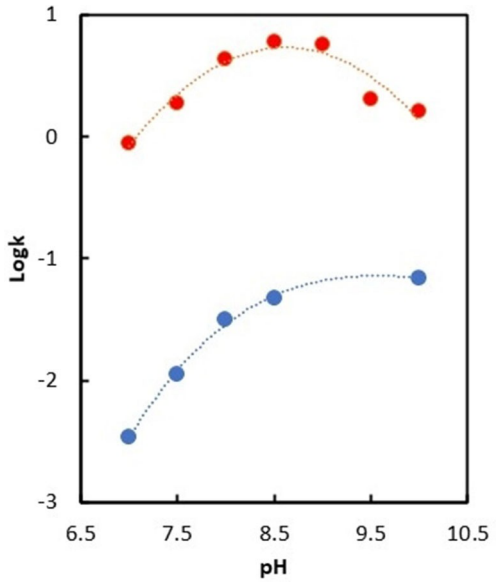

Figure 3. Dependence of the rate constant (k_2 for **HPNP** and k_{obs} for UPNP) from pH for the cleavage of **HPNP** and **UPNP** by **AuNP1**. The dotted lines refer to the interpolation of the points with two protonation constants for **HPNP**, red symbols, and a single protonation constant for **UPNP**, blue symbols. Data for **HPNP** from ref 13. Conditions for **UPNP**: [**AuNP1**] = 5×10^{-6} M, [**UPNP**] = 3.0×10^{-5} M, [buffers] = 1.0×10^{-2} M, T = 25 °C. Note that since the rate constants reported for the two substrates are different the two curves cannot be used to compare relative reactivities but only the profile of the pH dependence.

molecule. The resulting OH- is strongly bound to the metal ion thus inhibiting the binding of the substrate. The more tightly bound **UPNP** competes more favorably with the OH- for the coordination to Zn(II) and remains attached to the catalytic site also at high pH. Notably, catalyst **1** shows a single, catalytically relevant pK_a (7.8) in the cleavage of **HPNP**. Likely this is due to a higher pK_a for the water molecule bound to the second Zn(II) ion that falls beyond the pH interval studied.

The role of the pK_a of the leaving group

In addition to **UPNP**, we have studied five more uridine 3′-alkyl- and aryl-phosphodiesters (**3a**–**e**, Figure 1) to assess the role of the basicity of the leaving group in the **AuNP1**-catalyzed transesterification process. Reactions were performed at 40 °C and pH 7.5 in the presence of 5.0 μM **AuNP1**.The kinetics with the least reactive substrates (**3b**–**d**) could be followed by HPLC. In the case of **3a** the reaction was so slow that **AuNP1** decomposition became important and no reliable kinetic data could be obtained for this catalyst. The use of HPLC allowed us to follow the course of the reaction and monitor the final and intermediate products formed. Reaction rates for the far more reactive **UPNP** and **3e** substrates were determined from the extrapolation of the Arrhenius plots obtained from kinetics run at lower temperature and followed spectrophotometrically (see the Supporting Information). Analysis of the HPLC traces revealed the disappearance of the original uridine 3′-phosphate diesters, the intermediate formation of the cyclic phosphate (**2′,3′-cUMP**) which eventually formed two uridine monophosphates (**2′-UMP** and **3′-UMP**), see (a) in Scheme 1, with a clear preference for 2′O–P over 3′O–P bond cleavage. Analogously to what was reported for **1**,[28] no evidence of isomerization of the uridine 3′-phosphate diesters into the isomeric 2′-phosphates was obtained. This indicates that over the course of the transesterification process there is not enough stabilization of the transient cyclic phosphorane (Scheme 1 (b)) as, on the contrary, reported by Williams et al. for the dinuclear catalyst **2**.[29] This suggests that for **AuNP1** the conversion of the starting uridine 3′-phosphate diester into **2′,3′-cUMP** involves a single step in which nucleophile addition and leaving group departure are concerted (although not synchronous). The Brønsted plot, obtained at pH = 7.5 and 40 °C, reported in Figure 4 is linear in the entire interval of pK_a of the leaving groups explored (7.14–12.89) and gives a $\beta_{lg} = -0.86$. The same plot for catalysts **1** (pK_a interval 8.35–14.31), obtained by running the kinetics under the same conditions, is equally linear and gives $\beta_{lg} = -0.59$ (Figure 4).

This value is slightly lower than those reported for this catalyst under different conditions (−0.72 by Richard et al.[28] and −0.63 or −0.74 by Mikkola et al.[15] for aromatic and aliphatic leaving groups, respectively). The absence of any break in the linear plot for catalysts **1** and **AuNP1** indicates there is no change of mechanism for both of them. Williams et al.[29] reported, for a limited set of pK_a for catalyst **2**, a possible deviation from linearity at pK_a ca. 12.4, not significantly different from the value at which the break point for the OH-catalyzed process was reported.[30] At

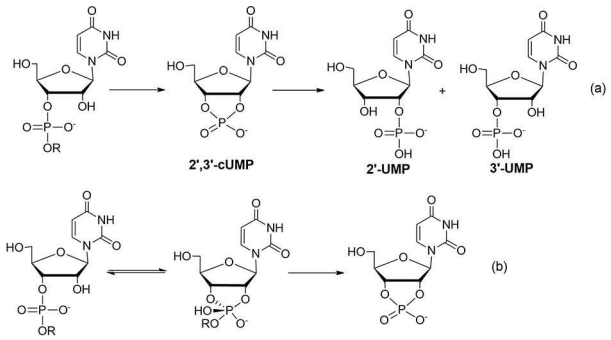

Scheme 1. (a) Products and intermediate formed in the cleavage of phosphates **3** by **AuNP1**. (b) Cleavage of uridine 3′-phosphates with the formation of a phosphorane intermediate.

Table 3. Bronsted parameters for the cleavage of uridine 3′-phosphate diesters in the presence of different catalysts.

Catalyst	β_{lg} (aromatic leaving groups)	β_{lg} (aliphatic leaving groups)	Reference
OH-	−1.34[a]	−0.52[a]	30
Zn(II)	−0.32[b,c]	−0.9[a,d]	33
AuNP1	−0.86[e]		This work
1	−0.59[e]		This work
	(−0.72,[f] −0.74[g] and −0.63[a,h,i])		15,28
2	−0.92 (−0.98)[j,k]	−0.43	29

[a] At 25 °C. [b] At 90 °C. [c] pH 5.6, [Zn(II)] = 10 mM. [d] pH 5.9, [Zn] = 10 mM. [e] pH = 7.5, 40 °C; [f] Conditions: pH 7.0, 25 °C. [g] pH 6.5, 50 °C. [h] pH 6.6. [i] With high and low pK_a, respectively. [j] Considering all substrates examined and two β_{lg}. [k] At 90 °C and pH 6.5.

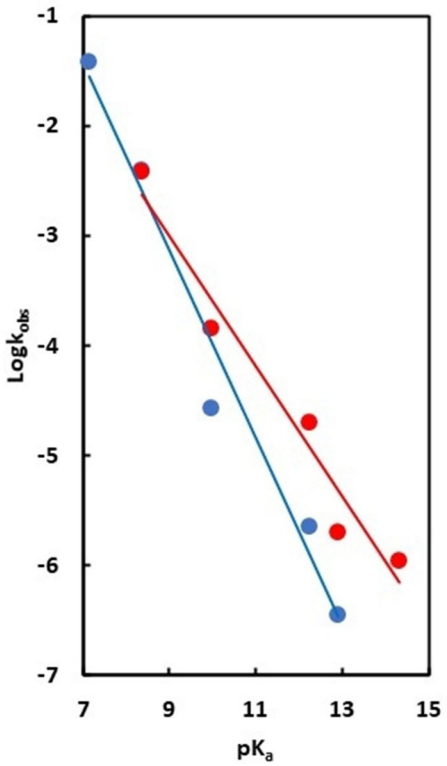

Figure 4. Brønsted plot for the cleavage of substrates **3** by catalysts **AuNP1** (blue symbols) and **1** (red symbols). Conditions: [**AuNP1**] = 5.0×10^{-6} M, [**1**] = 5.0×10^{-5} M, [**3**] = 3.0×10^{-5} M, [HEPES] = 0.01 M, pH 7.5, 40 °C. Note the difference in concentration of the two catalysts ([**1**] = 10 × [**AuNP1**].

higher pK_a of the leaving groups $\beta_{lg} = -1.34$ while with more acidic ones $\beta_{lg} = -0.52$ (estimated value). The β_{lg} for the different catalysts and the base-catalyzed, background reaction are reported in Table 3.

The mechanism of cleavage of uridine 3′-phosphate diesters by AuNP1

The analysis of Table 3 reveals a quite diverse picture for the cleavage of uridine 3′-phosphate diesters in the presence of dinuclear Zn(II) catalysts. This diversity was already pointed out by Mikkola et al. when analyzing a large collection of catalysts.[15] The base-catalyzed reaction indicates a mechanism ((b) in Scheme 1) in which an intermediate phosphorane is formed (analogously to the tetrahedral intermediate in carboxylate esters hydrolysis).[31] The break point of the Brønsted plot of the base-catalyzed process occurs at pK_a = 12.58. This value is close to that reported for the 2′ hydroxyl of uridine 3′-phosphate ethyl ester (12.85). This similarity is striking and resembles what one would expect for a quasi-symmetrical reaction (attack by the nucleophile/leaving group departure) despite being an intramolecular process. The base-catalyzed process, however, does not allow isomerization of the starting material to the 3′ derivative indicating the intermediate phosphorane is short-lived under these conditions. For catalyst **2** also the formation of a phosphorane intermediate was indicated but, in this case, it survives long enough to allow isomerization to occur. For this reason, it was suggested a strong interaction of the transition state with the dinuclear catalyst leading to significant dissipation of the developing negative charge in the reaction path towards this intermediate. Catalyst **2** binds so strongly to the phosphate to resemble a phosphate triester.[16,29,32] This facilitates the intramolecular nucleophilic attack and is consistent with the relatively rather negative β_{lg} (−0.92 for the less acidic leaving groups). The picture for catalyst **1** is different: no intermediate is formed, and the slope of the plot is less negative (−0.59 under the same conditions used for **AuNP1**). This implies a lower stabilization of the phosphorane but also a significant contribution to leaving group departure through proton transfer. **AuNP1** presents similarities with **1** and **2**. On one side it does not stabilize the phosphorane enough as is the case of catalyst **1**. On the other hand, its nucleophilic contribution to catalysis is important as for catalyst **2**. The better assistance in leaving group departure exerted by catalyst **1** compared to **AuNP1** results in an enhanced catalytic performance by the nanoparticles as the leaving groups become more acidic. The poorer stabilization of the phosphorane exerted by the nanoparticles may be the result of the partial detachment of the phosphate from the catalytic site required to allow the reaction to occur as suggested by the thermodynamic studies reported above. Thus, the presence of the nucleobase by increasing the stabilization of the ground state, not only negatively affects the efficiency of the catalytic process but also its mechanism. Nevertheless, **AuNP1** is still a better catalyst than **1**. Finally it should be pointed out that the behavior of all the above catalysts is different from that of aqueous Zn(II) (at slightly acidic pH to prevent precipitation).[33] Zn(II) catalysis provides in this case an important general acid catalysis contribution, particularly for the less acidic alcohols. The Brønsted plot shows $\beta_{lg} = -0.32$ and −0.9 for the less and more acidic leaving groups (alkyl and aryl derivatives), respectively. Accordingly, alkyl alcohols depart as neutral species while aryl derivatives depart as oxyanions. Notably, the proposed mechanism requires only a single metal ion contrary to catalysts **1**, **2** and **AuNP1** that are dinuclear ones.

Conclusion

We have compared AuNPs active in the cleavage of RNA model substrates and operating with a dinuclear mechanism with other two catalysts also based on a dinuclear catalytic site. The picture that emerges is quite diverse for the three catalytic systems. Catalyst **2** represents the extreme case of maximum stabilization of the phosphorane (Scheme 1 (b)) that forms in the transformation of the reagent into the cyclic product **2′,3′-cUMP**. This catalyst appears to be able to dissipate most of the charge developed during the evolution to products. Assistance in leaving group departure is possibly observed with this catalyst only for the more acidic alcohols (pK_a < 12.4). On the contrary catalyst **1** does not stabilize enough the phosphorane but provides significant assistance in leaving group departure. **AuNP1** share properties of both catalysts. On one side, as in the case of **1**, the phosphorane is not stabilized enough to become an intermediate. On the other, as in the case of **2** for the less acidic alcohols, little

assistance in leaving group departure is provided. The most important contribution to catalysis is hence nucleophilic.

It is interesting to note that, despite that **AuNP1** owe most of its efficiency to a high affinity for the uridine 3'-phosphate diesters (see Table 1), this is partly lost on the way to the transition state. Thus, although in principle it should behave like catalyst **2**, it fails to stabilize enough the transient phosphorane. The uridine moiety, while it is beneficial in stabilizing the ground state, is detrimental to reach the optimum geometry in the transition state. Neither catalyst **1** nor **2** appear to be able to interact with the uridine moiety of the substrates, likely because their catalytic sites are rather well defined and little flexible, contrary to that present on the monolayer passivating the gold nanoparticles. One may argue that better performing AuNPs could take advantage of the presence of cationic groups to assist the metal ion in the catalytic process as in the case of catalyst **2**. We have observed that this is indeed the case for very challenging substrates such as DNA.[10]

Our results show how very subtle changes, in both the catalyst and substrate, may significantly affect the mechanism of metal ion catalyzed cleavage of RNA phosphodiesters.

Acknowledgements

Funding from the European Union Framework Programme for Research and Innovation Horizon 2020 (H2020-MSCA-ITN-2016 MMBio – 721613) and Fondazione Cariparo ("Ricerca Scientifica di Eccellenza" Grant "SELECT") is gratefully acknowledged.

Conflict of Interest

The authors declare no conflict of interest.

Keywords: Brønsted plot · gold nanoparticles · metal ion catalysis · phosphate cleavage · RNA cleavage

[1] a) D. Desbouis, I. Troitsky, M. Belousoff, L. Spiccia, B. Graham, *Coord. Chem. Rev.* **2012**, *256*, 897–937; b) F. Mancin, P. Scrimin, P. Tecilla, *Chem. Commun.* 2012, 48, 5545–5559; c) F. Mancin, P. Scrimin, P. Tecilla, U. Tonellato, *Chem. Commun.* **2005**, 2540–2548.
[2] R. Wolfenden, *Annu. Rev. Biochem.* **2011**, *80*, 645–667.
[3] W. Yang, *Q. Rev. Biophys.* **2011**, *44*, 1–93.
[4] G. Palermo, A. Cavalli, M. L. Klein, M. Alfonso-Prieto, M. Peraro, M. De Vivo, *Acc. Chem. Res.* **2015**, *48*, 220–228.
[5] M. Diez-Castellnou, A. Martinez, F. Mancin, *Adv. Phys. Org. Chem.* **2017**, *51*, 129–186.
[6] J. Chin, *Acc. Chem. Res.* **1991**, *24*, 145–152.
[7] D. Desbouis, I. Troitsky, M. Belousoff, L. Spiccia, B. Graham, *Coord. Chem. Rev.* **2012**, *256*, 897–937.
[8] C. Fasting, C. A. Schalley, M. Weber, O. Seitz, S. Hecht, B. Koksch, J. Dernedde, C. Graf, E. Knapp, R. Haag, *Angew. Chem. Int. Ed.* **2012**, *51*, 10472–10498; *Angew. Chem.* **2012**, *124*, 10622–10498.
[9] P. Scrimin, M. Cardona, C. Prieto, L. J. Prins, *Multivalency as a Design Criterion in Catalyst Development, Ch. 7, Catalyst Development in Multivalency: Concepts, Research & Applications*, J. Huskens, L. J. Prins, R. Haag, B. J. Ravoo, Eds., John Wiley & Sons Ltd., **2017**.
[10] J. Czescik, S. Zamolo, T. Darbre, R. Rigo, C. Sissi, A. Pecina, L. Riccardi, M. D. Vivo, F. Mancin, P. Scrimin, *Angew. Chem. Int. Ed.* **2021**, *60*, 1423–1432; *Angew. Chem.* **2021**, *133*, 1443–1432.
[11] F. Mancin, L. Prins, P. Pengo, L. Pasquato, P. Tecilla, P. Scrimin, *Molecules* **2016**, *21*, 1014.
[12] a) F. Manea, F. B. Houillon, L. Pasquato, P. Scrimin, *Angew. Chem. Int. Ed.* **2004**, *43*, 6165; *Angew. Chem.* **2004**, *116*, 6291–6169; b) H. Wei, E. Wang, *Chem. Soc. Rev.* **2013**, *42*, 6060–6093; c) J. Wu, X. Wang, Q. Wang, Z. Lou, S. Li, Y. Zhu, L. Qin, H. Wei, *Chem. Soc. Rev.* **2019**, *48*, 1004–1076; d) L. Gabrielli, L. J. Prins, F. Rastrelli, F. Mancin, P. Scrimin, *Eur. J. Org. Chem.* **2020**, 5044–5055.
[13] J. Czescik, S. Zamolo, T. Darbre, F. Mancin, P. Scrimin, *Molecules* **2019**, *24*, 2814.
[14] S. Mikkola, T. Lönnberg, H. Lönnberg, *Beilstein J. Org. Chem.* **2018**, *14*, 803–837.
[15] H. Korhonen, T. Koivusalo, S. Toivola, S. Mikkola, *Org. Biomol. Chem.* **2013**, *11*, 8324–8339.
[16] H. Korhonen, N. H. Williams, S. Mikkola, *J. Phys. Org. Chem.* **2013**, *26*, 182–186.
[17] a) S. Aoki, E. Kimura, *Chem. Rev.* **2004**, *104*, 769–788; b) E. Kimura, H. Kitamura, K. Ohtani, T. Koike, *J. Am. Chem. Soc.* **2000**, *122*, 4668; c) M. Shionoya, E. Kimura, M. Shiro, *J. Am. Chem. Soc.* **1993**, *115*, 6730.
[18] M. Diez-Castellnou, F. Mancin, P. Scrimin, *J. Am. Chem. Soc.* **2014**, *136*, 1158–61.
[19] G. Zaupa, C. Mora, R. Bonomi, L. J. Prins, P. Scrimin, *Chem. Eur. J.* **2011**, *17*, 4879–89.
[20] L. Riccardi, L. Gabrielli, X. Sun, F. Biasi, F. Rastrelli, F. Mancin, M. De Vivo, *Chem* **2017**, *3*, 92–109.
[21] G. Guarino, F. Rastrelli, P. Scrimin, F. Mancin, *J. Am. Chem. Soc.* **2012**, *134*, 7200–7203.
[22] a) Q. Wang, H. Lönnberg, *J. Am. Chem. Soc.* **2006**, *128*, 10716–10728; b) Q. Wang, E. Leino, A. Jancsó, I. Szilágyi, T. Gajda, E. Hietamäki, H. Lönnberg, *ChemBioChem* **2008**, 9, 1739–1748; c) M. Laine, T. Lönnberg, M. Helkearo, H. Lönnberg, *Inorg. Chim. Acta* **2016**, *452*, 111–117.
[23] Y. Lyu, L. Morillas-Becerril, F. Mancin, P. Scrimin, *J. Hazard. Mater.* **2021**, *415*, 125644.
[24] A. Yatsimirsky, *Coord. Chem. Rev.* **2005**, *249*, 1997–2011.
[25] R. Cacciapaglia, S. D. Stefano, L. Mandolini, *Acc. Chem. Res.* **2004**, *37*, 113–122.
[26] M.-Y. Yang, J. P. Richard, J. R. Morrow, *Chem. Commun.* **2003**, 2832–2833.
[27] O. Iranzo, A. Y. Kovalevsky, J. R. Morrow, J. P. Richard, *J. Am. Chem. Soc.* **2003**, *125*, 1988–1993.
[28] J. R. Morrow, T. L. Amyes, J. P. Richard, *Acc. Chem. Res.* **2008**, *41*, 539–48.
[29] H. Korhonen, S. Mikkola, N. H. Williams, *Chem. Eur. J.* **2012**, *18*, 659–670.
[30] H. Lönnberg, R. Strömberg, A. Williams, *Org. Biomol. Chem.* **2004**, *2*, 2165–2167.
[31] P. Scrimin, P. Tecilla, U. Tonellato, *J. Org. Chem.* **1994**, *59*,10–24.
[32] M. Kosonen, K. Hakala, H. Lönnberg, *J. Chem. Soc. Perkin Trans. 2* **1998**, 663–670.
[33] S. Mikkola, E. Stenman, K. Nurmi, E. Yousefi-Salakdeh, R. Strömberg, H. Lönnberg, *J. Chem. Soc. Perkin Trans. 2* **1999**, 1619–1626.

Manuscript received: January 25, 2021
Accepted manuscript online: March 29, 2021
Version of record online: May 1, 2021

